Improved Image Navigation and Registration (INR) Algorithms

Ahmed Aly Kamel

Abstract Improved image navigation and registration algorithms are presented based on Kalman filter to allow near real-time delivery operation of level 1B data blocks and LRIT/HRIT subimages (instead of a whole image) to users. Kalman filter estimates attitude correction angles, orbit position relative to ideal geostationary orbit, and internal misalignments of imagers with single mirror or two mirrors. Kalman filter measurements consist of landmarks extracted from the imaging instrument level 1A data blocks, orbit maneuver delta V or coarse orbit from flight dynamics, and spacecraft inertial angular rate telemetry inserted in the imager wideband data. The state vector most significant improvement represents the effect of scan mirror axes orthogonality misalignment angle due to thermal variation and measurement errors. This improvement is shown to be in the north-south direction and equals to the orthogonality misalignment angle multiplied by the tangent of the east-west scan angle. The improved image navigation and registration algorithms are also applicable to systems with star and landmark measurements and systems with star only measurements.

Nomenclature

ABI	:	advanced baseline imager
ACF	:	attitude control frame
C	:	cosine
COMS	:	communication, ocean, and meteorological satellite
ECLF	:	earth centered local frame
EW	:	east-west
FDS	:	flight dynamics system
FGF	:	fixed grid frame
FPM	:	focal plane module
GOES	:	geostationary operational environmental satellite
GPS	:	global positioning system
HRIT	:	high rate information transmission
IIRF	:	instrument internal reference frame
IMC	:	image motion compensation
IMU	:	inertial measurement unit
INR	:	image navigation and registration
IOT	:	in orbit test
KF	:	Kalman filter
L	:	geocentric latitude
LOS	:	line of sight
LRIT	:	low rate information transmission

Ahmed Aly Kamel
Kamel Engineering Services, Los Angeles, USA, ahmed@kamelengineering.com

LRF : LOS reference frame
NS : north-south
O : orthogonality
OD : orbit determination
P : landmark or point on earth
ParSEC : parametric systematic error correction
R : radius
S : sine
SV : state vector
UTC : coordinated universal time
V : velocity
θ : pitch angle
λ : longitude
ϕ : roll angle
ψ : yaw angle

Subscripts

att : attitude
C : combined
corr : correction
eq : equator
m : misalignment or number of misalignments
0 : initial
S : spacecraft

1 Introduction

The purpose of this paper is to improve the generalized image navigation algorithm provided in Ref.[1] based on the improved misalignment equations provided in Ref. [2].

The term Image Navigation and Registration and the INR acronym were coined by Kamel [3] and patented in US patents # 4,688,091, 4,688,092, and 4,746,976 to represent a system that determines image pixel location and registers it to fixed grid. This original system was designed to meet GOES I-M (the first generation of 3-axis stabilized GOES satellites) requirements. IMC onboard spacecraft was used to meet three sigma navigation requirements of 112 microradians and three sigma registration requirements of 42 microradians.

The original INR invention became the foundation for subsequent GOES and similar systems worldwide[4-8]. The INR system requirements have been tightened as the spacecraft and ground systems hardware has been improved [9-15]. For example, the three sigma GOES N-P and COMS navigation requirements were tightened to 56 microradians and GOES-R navigation requirement was tightened to 21 microradians.

The image navigation part of INR relates to determining LOS absolute pointing. In this paper, this determination is performed for FGF originally used by Kamel [1] and became the standard for subsequent GOES[16].

Section 2 defines the INR and KF state vectors needed for the improved image navigation process for imagers with single mirror as well as imagers with two mirrors[13]

Section 3 describes the improved fundamental algorithm which is based on landmark measurements, inertial angular rate IMU telemetry, and orbit maneuvers delta V (or orbit with coarse accuracy) to determine attitude correction, orbit (or orbit refinement), and imager internal misalignments. COMS simulations [8] demonstrated that the fundamental algorithm meets the 56 microradians navigation requirement with margin.

Section 4 shows the effect of the improved misalignment equations due to the scan axes orthogonality angle O_m can be up to 0.2 O_m on image navigation and up to 0.3 O_m on within frame registration for single mirror instruments as well as for two mirror instruments.

The presented algorithms can be applied to systems with star measurements in addition or instead of landmark measurements. In this case, star measurements are used to determine attitude correction angles and imager misalignments, and landmark measurements are used to determine orbit (see Sect. 4.1 of Ref. [1]). If star measurements are used with no landmark measurements, orbit must be provided by FDS or GPS (see Sect. 4.2 of Ref. [1]). Finally, the presented algorithms can also be used for IMC onboard spacecraft like in Sect. 5 of Ref. [1] and for ground resampling like in Sect. 6 of Ref. [1].

2 Definitions

Section 2.1 defines the reference frames needed for transformation of LRF pixel coordinates (E_{LRF}, N_{LRF}) to its fixed grid coordinates (E_{FGF}, N_{FGF}). Section 2.2 defines the INR SV and KF SV needed for landmark residual computation shown in Fig. 1. Section 2.3 defines the time series approach used to determine the INR SV and KF SV values at a given time within the imagery data block.

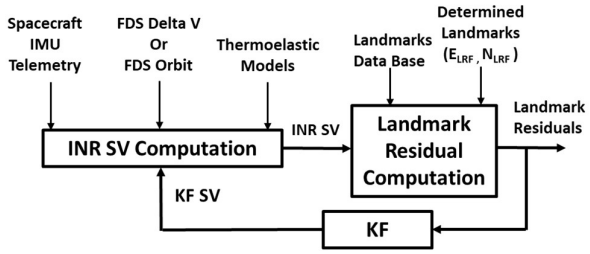

Fig. 1 INR and KF State Vectors Computations

2.1 Reference Frames

The reference frames are used for transformation of LOS coordinates from LRF to FGF.

LOS Reference Frame (LRF)

This frame is shown in Fig. 2 and it is attached to the instrument nadir position. The scan angles (E_{LRF}, N_{LRF}) are positive East and North where N_{LRF} is a rotation about X_{LRF} axis and E_{LRF} is a rotation about the rotated (dotted) Y-axis.

Instrument Internal Reference Frame (IIRF)

This frame is shown in Fig. 2 and it is attached near the instrument mounting frame to

spacecraft. Therefore, it is also called Virtual Instrument Mounting Frame (VIMF)[17] The (E_{IIRF}, N_{IIRF}) are positive East and North where N_{IIRF} is a rotation about X_{IIRF} axis and E_{IIRF} is a rotation about the rotated Y-axis.

Misalignments are produced by thermoelastic deformation. These misalignments and biases prevent IIRF axes to be ideally parallel to LRF axes. For single mirror instruments, (E_{IIRF}, N_{IIRF}) are determined from (E_{LRF}, N_{LRF}) and six misalignment angles($\phi_m, \theta_m, O_m, O_{m1}, O_{m2}, \psi_m$). For two mirror instruments [13], (E_{IIRF}, N_{IIRF}) are determined from (E_{LRF}, N_{LRF}) and four misalignment angles (O_m, O_{m1}, O_{m2}, ψ_m).

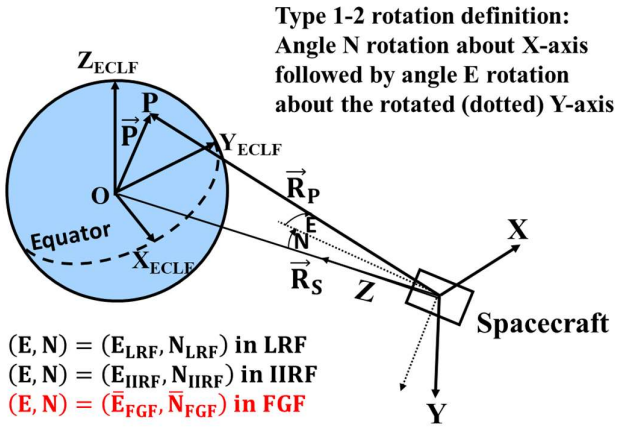

Fig. 2 LRF, IIRF, and FGF Coordinates Definitions

Attitude Control Frame (ACF)

This frame has its origin at the spacecraft center of gravity. Thermoelastic deformation and misalignment biases prevent ACF axes to be ideally parallel to the IIRF axes. Rotation angles of ACF relative to IIRF are defined as (roll, pitch, yaw) attitude correction angles (ϕ_{corr}, θ_{corr}, ψ_{corr}).

Fixed Grid Frame (FGF)

The FGF is shown in Figs. 2 to 5 and it defines the resampled image after orbit, attitude, and thermoelastic effects are removed. The fixed grid coordinates ($\bar{E}_{FGF}$, $\bar{N}_{FGF}$) are consistent with the parameters (λ, λ_0, ϕ_c, $-S_y$, $-S_z$, S_x, x, y) in Fig. 4.2.8 and section 4.2.8.2 of GOES-R Pug [16]. These parameters are the same as (λ_P, λ_{Si}, L_P, X_i, Y_i, Z_i, $\bar{E}_{FGF}$, $\bar{N}_{FGF}$) in Sect. 3.5.1 of this paper.

The ideal axes (X_i, Y_i, Z_i) represent FGF. The origin of these axes is aligned with the spacecraft ideal longitude λ_{Si} as shown in Figs. 3 and 4. Positive yaw Z-axis is oriented towards earth center, positive pitch Y-axis is oriented towards earth south direction, and X-axis forms a right-handed triad. The ideal axes (X_i, Y_i, Z_i) translate and rotate relative to IIRF. They are parallel to IIRF when (ϕ_C, θ_C, ψ_C) = (0,0,0) and they are the same as IIRF if the orbit translational part ($\Delta R_S/R_{Si}, \Delta\lambda_S, L_S$) is also = (0,0,0).

Earth Centered Local Frame (ECLF)

This frame is shown in Figs. 2 to 4 and its origin is at the center of the earth. Positive X_{ECLF} axis is oriented towards the spacecraft ideal longitude λ_{Si} as shown in Fig. 3,

positive Z_{ECLF} axis is oriented towards earth north direction, and positive Y_{ECLF} axis forms a right-handed triad.

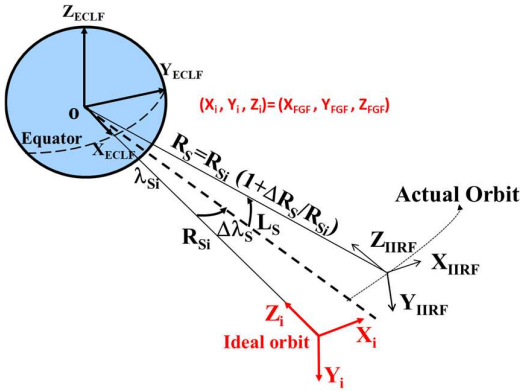

Fig. 3 Ideal FGF Translation Relative to IIRF

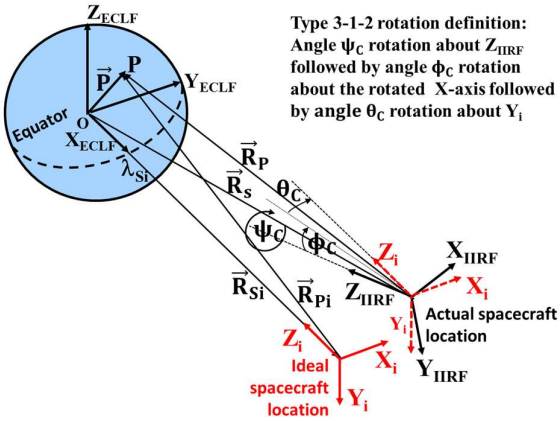

Fig. 4 Ideal FGF Translation and Rotation Relative to IIRF

2.2 INR State Vector

The SV_{INR} is required for pixel coordinate transformation from (E_{LRF}, N_{LRF}) to (E_{FGF}, N_{FGF}) as described in section 3.5.2. This is given by

$$SV_{INR} = [\, SV_C^T \quad SV_{orb}^T \; SV_m^T]^T \tag{1.1}$$

where

(X_i, Y_i, Z_i) are the same as $(X_{LRF}, Y_{LRF}, Z_{LRF})$ when $SV_{INR} = 0_{6+m}$.

SV_C is combined attitude state vector representing FGF axes orientation relative to IIRF.

SV_{orb} is orbit translation state vector representing FGF translation relative to IIRF.

SV_m is misalignment state vector representing IIRF misalignment relative to LRF.

$$SV_C = [\phi_C\ \theta_C\ \psi_C]^T = SV_{corr} + SV_{ACF} \quad (1.2)$$
$$SV_{corr} = [\phi_{corr}\ \theta_{corr}\ \psi_{corr}]^T = SV_{corr,model} + x_{corr} \quad (1.3)$$
$$SV_{ACF} = [\phi_{ACF}\ \theta_{ACF}\ \psi_{ACF}]^T \quad (1.4)$$
$$SV_{orb} = [\Delta R_S/R_{Si}\quad \Delta\lambda_S\quad L_S]^T \quad (1.5)$$
$$\Delta R_S/R_{Si} = (R_S - R_{Si})/R_{Si},\ \Delta\lambda_S = \lambda_S - \lambda_{Si} \quad (1.6)$$
$$SV_m = SV_{m,model} + x_m \quad (1.7)$$

and

$(SV_{corr,model}, SV_{m,model})$ are computed in section 3.10.

(x_{corr}, x_m) are defined in Eqs. (4.1), (4.2), and (5.2) and determined by KF.

R_S= spacecraft geosynchronous radius.

R_{Si} = ideal geostationary radius = 42164160 meters.

$(L_S, \lambda_S, \lambda_{Si})$ = spacecraft (geocentric latitude, longitude, ideal longitude)

$(\Delta R_S/R_{Si},\ \Delta\lambda_S,\ L_S)$ are called Kamel parameters [3,17,18] because they were originally used by Kamel [3] for GOES I-M [18] to represent actual orbit deviation from ideal geostationary orbit produced by spherical earth with no perturbations. In this paper, these parameters are determined by KF or by a combination of FDS orbit and refinement by KF. If FDS provides maneuver delta V

$$SV_{orb} = x_{orb} = \left[\delta R_s/R_s\quad \delta\lambda_s\quad \delta L_s\right]^T = \text{ideal orbit refinement by KF} \quad (2)$$

If FDS provides coarse orbit instead of delta V

$$SV_{orb} = [\Delta R_{FDS}/R_{Si}\quad \Delta\lambda_{FDS}\quad L_{FDS}]^T + x_{orb} \quad (3.1)$$

$$x_{orb} = \left[\delta R_s/R_s\quad \delta\lambda_s\quad \delta L_s\right]^T = \text{FDS orbit refinement by KF} \quad (3.2)$$

Now, SV_m in Eqs. (1.1) and (1.7) represents internal instrument misalignments as described in Sect. 2.1. For single mirror instruments, such as in GOES I-P, COMS, and MTSAT2, SV_m is given by Eq. (31.3) of Ref.[2]

$$SV_m = [\phi_m\ \ \theta_m\ \ O_m\ \ O_{m1}\ \ O_{m2}\ \ \psi_m]^T = SV_{m,model} + x_m \quad (4.1)$$

For two mirror instruments [13] such as in GOES-R, Himawari, and GK-2A, SV_m is given by Eq. (44.2) of Ref.[2]

$$SV_m = [O_m\ \ O_{m1}\ \ O_{m2}\ \ \psi_m]^T = SV_{m,model} + x_m \quad (4.2)$$

Kalman filter state vector

$SV_{KF} \equiv x$ is used for simplicity and it is given by

$$SV_{KF} \equiv x = [x_{corr}^T\ \dot{x}_{corr}^T\ x_{orb}^T\ \dot{x}_{orb}^T\ x_m^T\ \dot{x}_m^T]^T \quad (5.1)$$

$$x_{corr} = \delta SV_{corr},\ \dot{x}_{corr} = \text{constant}. \quad (5.2)$$

$$x_{orb} = \delta SV_{orb} = \left[\delta R_s/R_s\quad \delta\lambda_s\quad \delta L_s\right]^T,\ \dot{x}_{orb} = \delta\dot{SV}_{orb} = \left[\delta\dot{R}_s/R_s\quad \delta\dot{\lambda}_s\quad \delta\dot{L}_s\right]^T \quad (5.3)$$

$$x_m = \delta SV_m,\ \dot{x}_m = \text{constant}. \quad (5.4)$$

Now, Kalman filter state equation is based on attitude correction, orbit, and misalignment kinematics [see, e.g., Eq. (13-78) of Ref. [19], with u =0]

$$\dot{x} = Fx + w \tag{6.1}$$

F is state matrix and w is process noise vector

$$F = \begin{bmatrix} F_{corr} & 0_{6x6} & 0_{6x2m} \\ 0_{6x6} & F_{orb} & 0_{6x2m} \\ 0_{2mx6} & 0_{2mx6} & F_m \end{bmatrix}, F_{corr} = \begin{bmatrix} 0_{3x3} & I_{3x3} \\ 0_{3x3} & 0_{3x3} \end{bmatrix}, \quad F_m = \begin{bmatrix} 0_{mxm} & I_{mxm} \\ 0_{mxm} & 0_{mxm} \end{bmatrix} \tag{6.2}$$

$$F_{orb} = \begin{bmatrix} 0_{3x3} & I_{3x3} \\ \omega_e^2 F_{21} & 2\omega_e F_{22} \end{bmatrix}, F_{21} = \begin{bmatrix} 3 & 0 & 0 \\ 0 & 0 & 0 \\ 0 & 0 & -1 \end{bmatrix}, F_{22} = \begin{bmatrix} 0 & 1 & 0 \\ -1 & 0 & 0 \\ 0 & 0 & 0 \end{bmatrix} \tag{6.3}$$

ω_e= sidereal earth rotation rate = 7.2921159E-05 rad/sec (6.4)

F_{corr} and F_m are obtained from Eqs. (5.2) and (5.4) and F_{orb} is obtained from Euler-Hill's equations, e.g., Eq. (12.17) of Ref. [20], with n replaced by ω_e and $(x, y, z, \dot{x}, \dot{y}, \dot{z})$ replaced by $(\delta R_s/R_{si}, \delta\lambda_S, \delta L_S, \delta\dot{R}_s/R_{si}, \delta\dot{\lambda}_S, \delta\dot{L}_S)$.

2.3 State Vector Time Series

Landmark (or star) residual shown in Fig. 1 is computed using the INR state vector SV_{INR}. This requires evaluating SV_{INR} at a given time t_i from KF SV and the parameters shown in Fig. 1. This is done using linear interpolation and transition matrices.

For attitude telemetry time series spaced, e.g., at one second or 0.01 seconds and FDS orbit and thermoelastic models ($SV_{m,model}$, $SV_{corr,model}$) time series spaced, e.g., at one-minute, linear interpolation is used

$$y_i = y_0 + [(y_1 - y_0)/(t_1 - t_0)]\,(t_i - t_0) \quad t_0 \le t_i \le t_1 \tag{7}$$

where (y_0, t_0) and (y_1, t_1) are two successive points in the time series with $t_0 \le t_i \le t_1$ and (y_i, t_i) is the interpolated point.

State vector time series are spaced at times determined by landmark (or star) measurements which could be few minutes apart. In this case, its value at t_i is determined from its value at t_0 using transition matrix $A(\Delta t_i)$, $\Delta t_i = t_i - t_0$ as described in Sect. 3.3.

3 Improved Image Navigation Algorithm

Figure 5 shows KF flow for the fundamental INR algorithm. KF uses one landmark (or star) at a time to determine best (a-posteriori) state vector and state covariance matrix (x_1^+, P_1^+) estimate. KF is then re-initialized at t_1 to make propagation always between t_0 and t_1 and estimation at t_1.

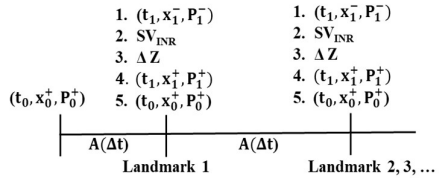

Fig. 5 Five-Step Kalman Filter Flow

3.1 Five-Step Kalman Filter Process

1. Compute a-priori state vector and state error covariance matrix (x_1^-, P_1^-) from (x_0^+, P_0^+) using the transition matrix $A(\Delta t)$ of Sect. 3.3 and process noise covariance matrix $Q(\Delta t)$ of Sect. 3.4 with $\Delta t = t_1 - t_0$. This is called state vector and covariance matrix propagation from t_0 and t_1

$$x_1^- = A(\Delta t)\, x_0^+, \;\; P_1^- = A(\Delta t)\, P_0^+ A(\Delta t)^T + Q(\Delta t) \tag{8}$$

2. Compute SV_{INR} from x_1^- using sections 2.2 and 2.3.
3. Compute landmark residual $\Delta Z = Z - \bar{Z}$ using section 3.5.
   If landmark is accepted because residual is within predetermined limit, go to step 4.
   If landmark is rejected because residual is outside the predetermined limit set $(t_1, x_1^+, P_1^+) = (t_1, x_1^-, P_1^-)$ and go to step 5.
4. Compute (x_1^+, P_1^+) from (x_1^-, P_1^-) and measurement model (H,R) of Sects. 3.6 and 3.7. This is called state vector and covariance matrix estimation at t_1

$$x_1^+ = x_1^- - K\Delta Z, \;\; K = P_1^- H^T (H P_1^- H^T + R)^{-1} \tag{9.1}$$

$$P_1^+ = (I - KH)\, P_1^- (I - KH)^T + KRK^T \tag{9.2}$$

where

x = KF state vector
I = identity matrix
K = Kalman gain obtained from minimizing the trace of the covariance matrix P_1^+.
$H = (\partial Z/\partial x)_{x=0}$ = landmark location sensitivity matrix.
Z = estimated landmark measurement $= Z_0 + H x + \varepsilon$.
Z_0 = Z evaluated at $x = \varepsilon = 0$ and ε = measurement noise vector, $E(\varepsilon) = 0$.
$R = E(\varepsilon\varepsilon^T)$, E denotes the expectation value.
$P_1^- = E[e_1^- (e_1^-)^T]$, $e_1^- = x - x_1^-$. $P_1^+ = E[e_1^+ (e_1^+)^T]$, $e_1^+ = x - x_1^+$.
Note that P_1^+ of Eq. (9.2) is used instead of the classical $P_1^+ = (I - KH)\, P_1^-$ to ensure P_1^+ remains positive definite and symmetric [see Eqs. 13-72 & 13-76 in Ref. [19]].

Note also that $(\Delta x_{corr}^+, \Delta x_{orb}^+, \Delta x_m^+) = (x_{corr}^+, x_{orb}^+, x_m^+) - (x_{corr}^-, x_{orb}^-, x_m^-)$ obtained from Eq. (9.1) can cause jumps in level 1B images at t_1. This can be avoided by adding its effect to $(\dot{x}_{corr}^+, \dot{x}_{orb}^+, \dot{x}_m^+)$ [also from Eq. (9.1)] by replacing it with $(\dot{x}_{corr}^+, \dot{x}_{orb}^+, \dot{x}_m^+) + (\Delta x_{corr}^+, \Delta x_{orb}^+, \Delta x_m^+)/\delta t$, where, δt = delta time, e.g., to next landmark (or star) or next KF event at t_1. After this slope adjustment, reset

$$(x_{corr}^+, x_{orb}^+, x_m^+)_{t_1} = (x_{corr}^-, x_{orb}^-, x_m^-)_{t_1} \tag{9.3}$$

5. Re-initialize KF at t_1 by setting $(t_0, x_0^+, P_0^+) = (t_1, x_1^+, P_1^+)$ to start the next cycle from t_0 to t_1.

3.2 Kalman Filter Initial Conditions

Kalman filter initial conditions (x_0^+, P_0^+) are needed to start KF at epoch t_0 as shown in Fig. 5. These, e.g., can be given by

$$x_0^+ = 0_{12+2m},\ P_0^+ = E[e_0^+(e_0^+)^T],\ e_0^+ = x_0 - x_0^+ = x_0 \tag{10.1}$$

$$P_0^+ = \begin{bmatrix} P_{corr,0}^+ & 0_{6x6} & 0_{6x2m} \\ 0_{6x6} & P_{orb,0}^+ & 0_{6x2m} \\ 0_{2mx6} & 0_{2mx6} & P_{m,0}^+ \end{bmatrix},\ P_{corr,0}^+ = \sigma_{corr,0}^2 \begin{bmatrix} I_{3x3} & 0_{3x3} \\ 0_{3x3} & 0_{3x3} \end{bmatrix}, \tag{10.2}$$

$$P_{orb,0}^+ = \sigma_{orb,0}^2 \begin{bmatrix} I_{3x3} & 0_{3x3} \\ 0_{3x3} & 0_{3x3} \end{bmatrix}, P_{m,0}^+ = \sigma_{m,0}^2 \begin{bmatrix} I_{mxm} & 0_{mxm} \\ 0_{mxm} & 0_{mxm} \end{bmatrix} \tag{10.3}$$

$(\sigma_{corr,0}, \sigma_{orbit,0}, \sigma_{m,0})$ are determined by error analysis.

I_{3x3}= 3x3 identity matrix, I_{mxm}= mxm identity matrix.

0_{3x3}= 3x3 null matrix, 0_{mxm}= mxm null matrix.

m= number of instrument internal misalignments.

3.3 Transition Matrix A

Kalman filter propagates the state vector via Eq. (8) with noise term omitted as shown by Eqs. (13-80) to (13-86) in Ref. [19]

$$x(t_i) = A(\Delta t_i)\, x(t_0)\ ,\ \Delta t_i = t_i - t_0, \qquad t_0 \le t_i \le t_1 \tag{11.1}$$

$$A(\Delta t_i) = \begin{bmatrix} A_{corr}(\Delta t_i) & 0_{6x6} & 0_{6x2m} \\ 0_{6x6} & A_{orb}(\Delta t_i) & 0_{6x2m} \\ 0_{2mx6} & 0_{2mx6} & A_m(\Delta t_i) \end{bmatrix} \tag{11.2}$$

A_{corr} and A_m are obtained from Eq. (6.2) and $A_{orb}(\Delta t_i)$ is obtained from Euler-Hill's equations, e.g., Eq. (12.18) of Ref. [20], with n replaced by ω_e, (x, y, z, $\dot{x}, \dot{y}, \dot{z}$) replaced by ($\delta R_s/R_{si}$, $\delta\lambda_S$, δL_S, $\delta\dot{R}_s/R_{si}$, $\delta\dot{\lambda}_S$, $\delta\dot{L}_S$), and $\omega_e\Delta t_i$ by γ

$$A_{corr}(\Delta t_i) = \begin{bmatrix} I_{3x3} & I_{3x3}\Delta t_i \\ 0_{3x3} & I_{3x3} \end{bmatrix}, A_m(\Delta t_i) = \begin{bmatrix} I_{mxm} & I_{mxm}\Delta t_i \\ 0_{mxm} & I_{mxm} \end{bmatrix} \tag{11.3}$$

$$A_{orb}(\Delta t_i) = \begin{bmatrix} A_{11} & A_{12} \\ A_{21} & A_{22} \end{bmatrix} \tag{11.4}$$

$$A_{11} = \begin{bmatrix} (4 - 3\,C_\gamma) & 0 & 0 \\ 6(S_\gamma - \gamma) & 1 & 0 \\ 0 & 0 & C_\gamma \end{bmatrix},\ A_{12} = \frac{1}{\omega_e}\begin{bmatrix} S_\gamma & 2\,(1 - C_\gamma) & 0 \\ -2(1 - C_\gamma) & (4S_\gamma - 3\gamma) & 0 \\ 0 & 0 & S_\gamma \end{bmatrix} \tag{11.5}$$

$$A_{21} = \begin{bmatrix} 3\,\omega_e S_\gamma & 0 & 0 \\ 6\omega_e(C_\gamma - 1) & 0 & 0 \\ 0 & 0 & -\,\omega_e S_\gamma \end{bmatrix},\ A_{22} = \begin{bmatrix} C_\gamma & 2\,S_\gamma & 0 \\ -2\,S_\gamma & (4C_\gamma - 3) & 0 \\ 0 & 0 & C_\gamma \end{bmatrix} \tag{11.6}$$

Where, C_x= Cos x, S_x= Sin x, and T_x= Tan x are used throughout this paper.

3.4 Process Noise Covariance Matrix Q

The process noise covariance matrix Q is obtained from the system modeling process noise vector w of Eq. (6.1) which is zero mean white noise assumed to be uncorrelated with the measurements noise vector ε of Eq. (22)

$$E[w(t)] = 0\ ,\ E[w(t)w(\tau)^T] = V(t)\delta_D(t - \tau) \tag{12.1}$$

where, $\delta_D$is the Dirac delta and V is known, symmetric, nonnegative definite matrix given by

$$V(t_0) = \begin{bmatrix} V_{corr,0} & 0_{6x6} & 0_{6x2m} \\ 0_{6x6} & V_{orb,0} & 0_{6x2m} \\ 0_{2mx6} & 0_{2mx6} & V_{m,0} \end{bmatrix}, V = \begin{bmatrix} V_{corr} & 0_{6x6} & 0_{6x2m} \\ 0_{6x6} & V_{orb} & 0_{6x2m} \\ 0_{2mx6} & 0_{2mx6} & V_m \end{bmatrix} \tag{12.2}$$

$$V_{y,0} = \begin{bmatrix} \sigma_{vo,y}^2 I_{3x3} & 0_{3x3} \\ 0_{3x3} & 0_{3x3} \end{bmatrix}, V_y = \begin{bmatrix} \sigma_{v,y}^2 I_{3x3} & 0_{3x3} \\ 0_{3x3} & \sigma_{u,y}^2 I_{3x3} \end{bmatrix} \tag{12.3}$$

y = corr, orb, or m. For m, 3 replaced by m.
σ_{vo}= measurement white noise standard deviation, rad.
σ_v= random walk standard deviation, rad/sec$^{1/2}$.
σ_u= rate random walk standard deviation, rad/sec$^{3/2}$.

Now, Eqs. (13-79), (13-83) and (13-89) of Ref. [19], lead to

$$Q(\Delta t) = V(t_0) + \int_{t_0}^{t} A(t,\tau)\, V(\tau) A(t,\tau)^T d\tau \tag{13.1}$$

Substituting $A \cong I + F(t-\tau)$ in above equation leads to

$$Q(\Delta t) = V(t_0) + V\Delta t + \frac{1}{2}[FV + VF^T]\Delta t^2 + \frac{1}{3} FVF^T \Delta t^3 \tag{13.2}$$

This leads to the closed form process noise covariance matrix

$$Q(\Delta t) = \begin{bmatrix} Q_{corr} & 0_{6x6} & 0_{6x2m} \\ 0_{6x6} & Q_{orb} & 0_{6x2m} \\ 0_{2mx6} & 0_{2mx6} & Q_m \end{bmatrix} \tag{13.3}$$

Where

$$Q_y = \begin{bmatrix} \left(\sigma_{vo,y}^2 + \sigma_{v,y}^2 \Delta t + \frac{1}{3}\sigma_{u,y}^2 \Delta t^3\right) I_{3x3} & \frac{1}{2}\sigma_{u,y}^2 \Delta t^2 I_{3x3} \\ \frac{1}{2}\sigma_{u,y}^2 \Delta t^2 I_{3x3} & \sigma_{u,y}^2 \Delta t\, I_{3x3} \end{bmatrix} \tag{13.4}$$

y = corr, orb, or m. For m, I_{3x3} is replaced by I_{mxm}.

Note that the first element of the above matrix is the same as Eq. (7-143) in Ref. [19], which can be evaluated at, e.g., Δt = (1, 120, 300) seconds to solve for (σ_{vo}, σ_v, σ_u) from 3 equations in 3 unknowns.

3.5 Landmark Residual Computation

The landmark residual $\Delta Z = Z - \bar{Z}$ is needed for step 3 of Sect. 3.1 and it is computed in the next two subsections [see Eqs. (15.1) and (20.3)].

3.5.1 Actual Landmark Measurement Computation

In view of Figs. 2 and 4 and using unit vector components along (X_i, Y_i, Z_i) fixed grid axes, we get

$$\vec{R}_{Pi} = \vec{P} - \vec{R}_{Si}\ , \vec{R}_{Pi} = R_{Pi}\hat{R}_{Pi}, \vec{P} = (R_e + h)\hat{P}, \vec{R}_{Si} = R_{Si}\hat{R}_{Si} \tag{14.1}$$

Where

$$\widehat{R}_{Pi,FGF} = \begin{bmatrix} \widehat{R}_{Pi,Xi} \\ \widehat{R}_{Pi,Yi} \\ \widehat{R}_{Pi,Zi} \end{bmatrix} = \begin{bmatrix} S_{\overline{E}_{FGF}} \\ -C_{\overline{E}_{FGF}} S_{\overline{N}_{FGF}} \\ C_{\overline{E}_{FGF}} C_{\overline{N}_{FGF}} \end{bmatrix}, \widehat{P}_{FGF} = \begin{bmatrix} C_{L_P} S_{\Delta\lambda_P} \\ -S_{L_P} \\ -C_{L_P} C_{\Delta\lambda_P} \end{bmatrix}, \widehat{R}_{Si,FGF} = \begin{bmatrix} 0 \\ 0 \\ -1 \end{bmatrix} \quad (14.2)$$

$$R_e = R_{eq}\left(1 + a_e S_{L_P}^2\right)^{-\frac{1}{2}}, a_e = (1-f)^{-2} - 1 \cong 2f \ , \Delta\lambda_P = \lambda_P - \lambda_{Si} \quad (14.3)$$

And

R_{eq} = equatorial radius = 6378137 meters, f = earth flattening=1/298.257222096.
L_P = landmark geocentric latitude, λ_P = landmark longitude.
h = landmark height.

This leads to the landmark coordinates to be stored in the landmark database

$$\overline{Z} = [\overline{E}_{FGF} \quad \overline{N}_{FGF}]^T \quad (15.1)$$

$$\overline{E}_{FGF} = \sin^{-1}\left[(R_e + h)C_{L_P} S_{\Delta\lambda_P} / R_{Pi}\right] \quad (15.2)$$

$$\overline{N}_{FGF} = \tan^{-1}\left[\{(R_e + h)S_{L_P}\} / \{R_{Si} - (R_e + h)C_{L_P} C_{\Delta\lambda_P}\}\right] \quad (15.3)$$

Where,

$$R_{Pi} = \left|\vec{R}_{Pi}\right| = \left|\vec{P} - \vec{R}_{Si}\right| = \left[(R_e + h)^2 + R_{Si}^2 - 2R_{Si}(R_e + h)C_{L_P} C_{\Delta\lambda_P}\right]^{\frac{1}{2}} \quad (15.4)$$

3.5.2 Estimated Landmark Measurement

Estimated fixed grid coordinates (E_{FGF}, N_{FGF}) are obtained from (E_{LRF}, N_{LRF}) of Fig. 2 and SV_{INR} of Eq. (1) as shown in the next four subsections.

3.5.2.1 LRF to IIRF Transformation

The unit vector $\widehat{R}_P$ components in IIRF is given by Fig. 2.

$$\widehat{R}_{P,IIRF} = \left[S_{E_{IIRF}} \vdots -C_{E_{IIRF}} \ S_{N_{IIRF}} \vdots \ C_{E_{IIRF}} \ C_{N_{IIRF}}\right]^T \quad (16.1)$$

The transformation from (E_{LRF}, N_{LRF}) to (E_{IIRF}, N_{IIRF}) is given by Eqs. (6), (7.2), (7.3), (31.1) to (31.3), (38.1), (44.1), and (44.2) of Ref. [2]:

$$\begin{bmatrix} E_{IIRF} \\ N_{IIRF} \end{bmatrix} = \begin{bmatrix} E_{LRF} \\ N_{LRF} \end{bmatrix} - h_m SV_m \quad (16.2)$$

For single mirror instruments, FPM rotates by the angle N and

$$\begin{bmatrix} E_{LRF} \\ N_{LRF} \end{bmatrix} = \begin{bmatrix} \mathrm{Sin}^{-1}(cS_E + AC_E) \\ \mathrm{Tan}^{-1}\left(\frac{cS_N C_E - AS_N S_E + BC_N}{cC_N C_E - AC_N S_E - BS_N}\right) \end{bmatrix} \quad (16.3)$$

$$c = \sqrt{1 - a^2 - b^2}, A = a\,C_N + b\,S_N, B = b\,C_N - a\,S_N \quad (16.4)$$

$$h_m = \begin{bmatrix} -S_N \ \vdots \ 0 \ \vdots \ 0 \vdots \ 0 \ \vdots 1 - C_N \ \vdots \ B \\ 1 - \frac{C_N}{C_E} \vdots \frac{S_N}{C_E}(1 + S_E) \vdots T_E \vdots (1 - C_E)/C_E \vdots \ -T_E S_N \vdots -A \end{bmatrix} \quad (16.5)$$

$$SV_m = [\phi_m \ \ \theta_m \ \ O_m \ \ O_{m1} \ \ O_{m2} \ \ \psi_m]^T \quad (16.6)$$

And

(E, N) = optical (East, North) scan angles = (2e, n)

(e, n) = mechanical (east, north) scan angles.

(a, b) = (E, N) detector LOS location relative to FPM center.

For two mirror instruments, FPM reflected image does not rotate and

$$\begin{bmatrix} E_{LRF} \\ N_{LRF} \end{bmatrix} = \begin{bmatrix} \mathrm{Sin}^{-1}(cS_E + aC_E) \\ \mathrm{Tan}^{-1}\left(\frac{cS_NC_E - aS_NS_E + bC_N}{cC_NC_E - aC_NS_E - bS_N}\right) \end{bmatrix} \tag{17.1}$$

$$h_m = \begin{bmatrix} 0 & \vdots & 0 & \vdots & 1 - C_N & \vdots & b \\ T_E & \vdots & (1 - C_E)/C_E & \vdots & -T_ES_N & \vdots & -a \end{bmatrix} \tag{17.2}$$

$$SV_m = [O_m \;\; O_{m1} \;\; O_{m2} \;\; \psi_m]^T \tag{17.3}$$

And (E, N) = (2e, 2n)

It should be mentioned that (O_m , O_{m1}, O_{m2}, ψ_m) = (Orthogonality, Orthogonality1, Orthogonality2, Yaw) misalignment state vector was first introduced by Kamel during his INR support (2005-2008) of GOES-R ABI implementation phase at ITT.

Note that, inverse transformation to get (E_{LRF}, N_{LRF}) from (E_{IIRF}, N_{IIRF}) using Eq. (16.2) is needed to search for landmarks in level 1A data when IMC is off (or generate star LOS commands when IMC is off) from their (E_{FGF}, N_{FGF}) coordinates of Eq. (18.2). This can be obtained by substituting (E, N) = (E_{IIRF}, N_{IIRF}) and (a, b) = (0,0) in Eqs. (16.4) and (16.5) for single mirror instruments or in Eq. (17.2) for two mirror instruments. Note also that the misalignment state vector dimension = 6 for single mirror instruments and = 4 for two mirror instruments. This is because in single mirror instruments, the FPM reflected image rotates by the NS angle N while in the two mirror instruments, the FPM reflected image does not rotate.

Because $\sqrt{E_{LRF}^2 + N_{LRF}^2} \leq 8.7°$, the effect of (1-$C_E$) and/or (1-$C_N$) terms in h_m on INR performance could be insignificant. Also, because (a, b) are small, ψ_m effect could be insignificant. In this case, only orthogonality misalignment O_m is used [14,17] and the number of misalignments m=3 for single mirror and =1 for two mirrors. This suggests that KF INR software design should be based on deleting O_{m1} and/or O_{m2} in addition to ψ_m if proven to be insignificant by analysis and/or during IOT.

It should be mentioned that the yaw misalignment state ψ_m determination requires star and/or landmark measurements to be located at maximum separation from the FPM center. This is because the measurement residuals are not sensitive to $\psi_m$for measurements at the FPM center (i.e., a = b = 0). If this complicates INR operation, a special on orbit test (or inspection of level 1B swath to swath imagery data) can determine $\psi_m$bias (i.e., constant term). The use of this bias in Eqs. (16.6) or (17.3) should at least reduce (but not eliminate) ψ_m effect on INR performance. The special test consists of sighting a star (or a landmark) 3 times. The first time t_1 determines the location of the star (or landmark) within the FPM, second time t_2 makes the star (or landmark) located near the extreme south of the FPM, and third time t_3 makes the star (or landmark) located near the extreme north of FPM. The $\psi_m$bias is then computed from $\psi_m = (E_3 - E_2)/(N_3 - N_2)$, where (E_2, E_3) are the second and third star (or landmark) EW locations and (N_2, N_3) are the corresponding NS locations. Note that the third measurement must be rectified to the time

of the second measurement. This rectification is performed using spacecraft attitude telemetry and orbit knowledge to subtract spacecraft attitude and orbit effects on star (or landmark) motion relative to spacecraft between t_2 to t_3.

3.5.2.2 IIRF to FGF Transformation

The transformation of $\hat{R}_{P,IIRF}$ components of Eq. (16.1) to $\hat{R}_{P,FGF}$ is given by

$$\hat{R}_{P,FGF} = \left[\hat{R}_{P,Xi} \quad \hat{R}_{P,Yi} \quad \hat{R}_{P,Zi}\right]^T = M\,\hat{R}_{P,IIRF} \tag{18.1}$$

$$\hat{R}_{P,IIRF} = M^T \hat{R}_{P,FGF} \text{ for inverse transformation.} \tag{18.2}$$

The matrix M rotation is type 3-1-2 as shown in Fig. 4. Using Appendix E, Table E-1 of Ref. [19], and replacing (ϕ, θ, ψ) with $(\psi_C, \phi_C, \theta_C)$ shown in Fig. 4, we get

$$M = \begin{bmatrix} C_\theta C_\psi - S_\theta S_\phi S_\psi & C_\theta S_\psi + S_\theta S_\phi C_\psi & -S_\theta C_\phi \\ -S_\psi C_\phi & C_\psi C_\phi & S_\phi \\ S_\theta C_\psi + C_\theta S_\phi S_\psi & S_\theta S_\psi - C_\theta S_\phi C_\psi & C_\phi C_\theta \end{bmatrix}_C \tag{18.3}$$

3.5.2.3 R_P, λ_P, L_P Computation

In view of Figs. 3 and 4, Eqs. (14.1) (14.2), we get

$$\vec{P} = \vec{R}_S + \vec{R}_P,\ \vec{P} = (R_e + h)\hat{P},\ \vec{R}_S = R_S\hat{R}_S,\ \vec{R}_P = R_P\hat{R}_P \tag{19.1}$$

$$\hat{P}_{FGF} = \begin{bmatrix} C_{L_P} S_{\Delta\lambda_P} \\ -S_{L_P} \\ -C_{L_P} C_{\Delta\lambda_P} \end{bmatrix},\ \hat{R}_{S,FGF} = \begin{bmatrix} C_{L_S} S_{\Delta\lambda_S} \\ -S_{L_S} \\ -C_{L_S} C_{\Delta\lambda_S} \end{bmatrix},\ \hat{R}_{P,FGF} = \begin{bmatrix} \hat{R}_{P,Xi} \\ \hat{R}_{P,Yi} \\ \hat{R}_{P,Zi} \end{bmatrix} = M\hat{R}_{P,IIRF} \tag{19.2}$$

and R_P is obtained from

$$\left|\vec{P}\right| = \left|\vec{R}_S + \vec{R}_P\right| = \left|R_S\hat{R}_s + R_P\hat{R}_P\right| \rightarrow (R_e + h)^2 = R_S^2 + R_P^2 - 2R_P R_S C_{\alpha_s}$$

$C_{\alpha_s} = -$dot product of $\hat{R}_S$ and $\hat{R}_P = -\hat{R}_{P,Xi} C_{L_S} S_{\Delta\lambda_S} + \hat{R}_{P,Yi} S_{L_S} + \hat{R}_{P,Zi} C_{L_S} C_{\Delta\lambda_S}$

Solution of the above quadratic equation in R_P leads to

$$R_P = \frac{R_S}{r},\ r = \left[C_{\alpha_s} - \sqrt{C_{\alpha_s}^2 - C_{\alpha_e}^2}\right]^{-1},\ C_{\alpha_e}^2 = 1 - \left[(R_e + h)/R_S\right]^2 \tag{19.3}$$

Where

$R_e = R_{eq}\left(1 + a_e S_{L_P}^2\right)^{-\frac{1}{2}}$, R_{eq} and a_e are obtained from Eq. (14.3)

$(S_{L_P}, \lambda_P, L_P)$ obtained from Eqs. (19.1) and (19.2)

$$S_{L_P} = R_S(S_{L_S} - \hat{R}_{P,Yi}/r)/(R_e + h),\ L_P = \mathrm{Sin}^{-1}[R_S(S_{L_S} - \hat{R}_{P,Yi}/r)/(R_e + h)] \tag{19.4}$$

$$\lambda_P = \lambda_{Si} + \Delta\lambda_P = \lambda_{Si} + \mathrm{Tan}^{-1}[(r\,C_{L_S}S_{\Delta\lambda_S} + \hat{R}_{P,Xi})/(r\,C_{L_S}C_{\Delta\lambda_S} - \hat{R}_{P,Zi})] \tag{19.5}$$

Note that because $a_e \cong 0.007$ in the R_e equation, accurate R_e and r values should be obtained using couple of iterations starting with $R_e = R_{eq}$ on the right side of the r and S_{L_P} equations. Note also that $\sqrt{C_{\alpha_s}^2 - C_{\alpha_e}^2}$ is imaginary when $C_{\alpha_s}^2 < C_{\alpha_e}^2$. This indicates that LOS (E_{LRF}, N_{LRF}) correspond to a point outside Earth and the transition from Earth to space is undefined. This can be avoided if a fictitious earth with $C_{\alpha_e} = C_{\alpha_s}$ is used in Eq. (19.3) for the space portion of earth images. In this case, Eq. (19.3) reduces to

$$R_P = R_S C_{\alpha_s},\ r = 1/C_{\alpha_s} \tag{19.6}$$

3.5.2.4 Fixed Grid Coordinates Computation

In view of Figs. 2 and 4 and using Eqs. (14.1), (14.2), (19.1), and (19.2), we get

$$\vec{R}_{Pi} = \vec{R}_P + \vec{R}_S - \vec{R}_{Si} \tag{20.1}$$

$$\hat{R}_{Pi,FGF} = \begin{bmatrix} \hat{R}_{Pi,Xi} \\ \hat{R}_{Pi,Yi} \\ \hat{R}_{Pi,Zi} \end{bmatrix} = \frac{R_P}{R_{Pi}}\{M\hat{R}_{P,IIRF} + r[\hat{R}_{S,FGF} - \frac{R_{Si}}{R_S}\hat{R}_{Si,FGF}]\} = \begin{bmatrix} S_{E_{FGF}} \\ -C_{E_{FGF}} S_{N_{FGF}} \\ C_{E_{FGF}} C_{N_{FGF}} \end{bmatrix} \tag{20.2}$$

$$Z = \begin{bmatrix} E_{FGF} \\ N_{FGF} \end{bmatrix} = \begin{bmatrix} Sin^{-1}(\hat{R}_{Pi,Xi}) \\ -Tan^{-1}(\hat{R}_{Pi,Yi}/\hat{R}_{Pi,Zi}) \end{bmatrix} \tag{20.3}$$

Note that for star measurements, $\vec{R}_S - \vec{R}_{Si}$ is insignificant compared to $\vec{R}_P$ in Eq. (20.1) and, therefore, $\hat{R}_{Pi,FGF} = \hat{R}_{P,FGF}$ and Z is directly obtained from Eq. (18.1) and Sect. 3.5.2.3 is skipped.

3.6 Landmark Location Sensitivity Matrix H

The matrix H is used in step 4 of Sect. 3.1

$$H = (\frac{\partial Z}{\partial x})_{x=0} = [H_{corr} \quad H_{orb} \quad H_m],\ H_y = \left[\left(\frac{\partial Z}{\partial SV_y}\frac{\partial SV_y}{\partial x_y}\right)_{x_y=0} \quad 0_{2xn}\right] \tag{21.1}$$

Where y = corr, orb, or m and n=3 for y = corr and orb and n = m for y = m. The matrix H is obtained from the first and second rows of Eq. (20.2) with matrix M of Eq. (18.3) and $\hat{R}_{S,FGF}$ of Eq. (19.2) linearized using (sin δζ, cos δζ) ≅ (δζ, 1). SV_{INR} is obtained in terms of x from Eqs. (1.1) to (5.4). Substituting Eqs. (14.2), Eq. (16.1), and (19.2) in Eq. (20.2), we get

$$R_{Si}/R_S \cong 1 - \Delta R_S/R_{Si} \tag{21.2}$$

$$R_P/R_{Pi} \cong 1 - r\left[C_{E_{IIRF}} C_{N_{IIRF}} \vdots -S_{E_{IIRF}} \vdots -C_{E_{IIRF}} S_{N_{IIRF}}\right]SV_{orb} \tag{21.3}$$

$$\begin{bmatrix} S_{E_{FGF}} \\ -C_{E_{FGF}}S_{N_{FGF}} \end{bmatrix} \cong \begin{bmatrix} S_{E_{IIRF}} \\ -C_{E_{IIRF}}S_{N_{IIRF}} \end{bmatrix} + G_C SV_C + rG_{orb}SV_{orb} \tag{21.4}$$

$$G_C = -C_{E_{IIRF}}\begin{bmatrix} 0 & C_{N_{IIRF}} & S_{N_{IIRF}} \\ -C_{N_{IIRF}} & 0 & T_{E_{IIRF}} \end{bmatrix} \tag{21.5}$$

$$G_{orb} = \begin{bmatrix} C_{E_{IIRF}} C_{N_{IIRF}}S_{E_{IIRF}} & C^2_{E_{IIRF}} & -S_{N_{IIRF}}S_{E_{IIRF}}C_{E_{IIRF}} \\ -C^2_{IIRF}C_{N_{IIRF}} \ S_{N_{IIRF}} & C_{E_{IIRF}}S_{E_{IIRF}} \ S_{N_{IIRF}} & -(1 - C^2_{E_{IIRF}}S^2_{N_{IIRF}}) \end{bmatrix} \tag{21.6}$$

Where, SV_C is form Eq. (1.2) and SV_{orb} from Eq. (1.5).

Now, the partial derivatives of Eq. (21.4) w.r.t. y and using Eq. (16.2) for the partial derivatives of (E_{IIRF}, N_{IIRF}) w.r.t. x_m lead to the H matrix of Eq. (21.1). Note that $\partial SV_y/\partial x_y = I$. This leads to

1. H_{corr} is due to partial derivatives w.r.t. $(x_{corr}, \dot{x}_{corr})$ of Eqs. (1.2), (1.3), and (5.2)

$$H_{corr} = -[h_{corr} \quad 0_{2x3}],\ h_{corr} = \begin{bmatrix} 0 & C_N & S_N \\ 1 & T_E S_N & -T_E C_N \end{bmatrix}, T_E = S_E/C_E \quad (21.7)$$

   $(E, N) \cong (\overline{E}_{FGF}, \overline{N}_{FGF})$ of Eq. (15.1) (i.e., from landmark or star database).
2. H_{orb} is due to partial derivatives w.r.t. $(x_{orb}, \dot{x}_{orb})$ of Eqs. (2), (3.1) and (5.3)

$$H_{orb} = -[h_{orb} \quad 0_{2x3}],\ h_{orb} = -\bar{r}\begin{bmatrix} S_E C_N & C_E & -S_E S_N \\ S_N/C_E & 0 & C_N/C_E \end{bmatrix} \quad (21.8)$$

   Where,
   $\bar{r} = R_{Si}/R_{Pi} = [C_{\bar{\alpha}_S} - (C^2_{\bar{\alpha}_S} - C^2_{\bar{\alpha}_e})^{1/2}]^{-1}$
   $C_{\bar{\alpha}_S} = C_E C_N,\ C^2_{\bar{\alpha}_e} = 1 - [(R_e + h)/R_{Si}]^2,\ (E, N) \cong (\overline{E}_{FGF}, \overline{N}_{FGF})$
   R_e = earth radius from Eq. (14.3) evaluated at landmark geocentric latitude L_P from the landmark database.
   Note that for star measurements, R_{Si} is insignificant compared to R_{Pi} and, therefore, $\bar{r} \cong 0$. This indicates that star measurement residuals are insensitive to orbit translation and orbit must be determined either using landmark measurements or by FDS using ground ranging or GPS receiver on board spacecraft.
3. H_m is due to partial derivatives w.r.t. $(x_m, \dot{x}_m)$ of Eqs. (4.1), (4.2), and (5.4)

$$H_m = -[h_m \quad 0_{2xm}],\ h_m = \begin{bmatrix} C_{11} & \dots & C_{1m} \\ C_{21} & \dots & C_{2m} \end{bmatrix} \quad (21.9)$$

   Where $3 \le m \le 6$ for single mirror instruments and $1 \le m \le 4$ for two mirrors instruments as described in Sect. 3.5.2.1.

3.7 Landmark Measurement Noise Covariance Matrix R

The matrix R is used in step 4 of Sect. 3.1

$$R = E(\varepsilon\varepsilon^T) = \sigma_M^2 I_{2x2},\ \sigma_M^2 = \sigma^2_{positon} + \sigma^2_{match} \quad (22)$$

ε = measurement noise vector
σ_M= landmark measurement one sigma error.
$\sigma_{position}$= position error within the data base.
σ_{match} = matching error of landmark chip to imagery data.

3.8 Attitude Computation from Inertial Angular Rate Telemetry

The spacecraft inertial angular rates $(\omega_{sx}, \omega_{sy}, \omega_{sz})$ provided in wideband data every Δt_{att} seconds (e.g., 0.01 seconds) can be directly used to determine SV_{ACF} of Eq. (1.2). The rate $\dot{SV}_{ACF}$ is determined from $(\omega_{sx}, \omega_{sy}, \omega_{sz})$ using Fig. 4 with IIRF and $(\phi, \theta, \psi)_C$ replaced by ACF and $(\phi, \theta, \psi)_{ACF}$. Starting with $\dot{\theta}_{ACF} + \omega_e$ about $-Y_i$ axis, followed by $\dot{\phi}_{ACF}$ about the new $-X$ axis, and ending with $\dot{\psi}_{ACF}$ about $-Z_{ACF}$ axis and using M^T of Eq. (18.2), we get

$$\begin{bmatrix}\omega_{sx}\\ \omega_{sy}\\ \omega_{sz}\end{bmatrix} = -\dot{\psi}_{ACF}\begin{bmatrix}0\\0\\1\end{bmatrix} - \dot{\phi}_{ACF}\begin{bmatrix}C_\psi\\ S_\psi\\ 0\end{bmatrix}_{ACF} - (\dot{\theta}_{ACF} + \omega_e)\begin{bmatrix}-S_\psi C_\phi\\ C_\psi C_\phi\\ S_\phi\end{bmatrix}_{ACF} \quad (23.1)$$

This leads to

$$\dot{SV}_{ACF} = \begin{bmatrix}\dot{\phi}\\ \dot{\theta}\\ \dot{\psi}\end{bmatrix}_{ACF} = -\begin{bmatrix}\omega_{sy}S_\psi + \omega_{sx}C_\psi\\ \omega_e + (\omega_{sy}C_\psi - \omega_{sx}S_\psi)/C_\phi\\ \omega_{sz} - (\omega_{sy}C_\psi - \omega_{sx}S_\psi)S_\phi/C_\phi\end{bmatrix}_{ACF} \quad (23.2)$$

Now, SV_C of Eqs. (1.2) and (1.3) is re-defined to separate $SV_{corr,model}$

$$SV_C = \widetilde{SV}_C + SV_{corr,model},\ \widetilde{SV}_C = SV_{ACF} + x_{corr},\ \dot{\widetilde{SV}}_C = \dot{SV}_{ACF} + \dot{x}_{corr} \quad (23.3)$$

And the $\widetilde{SV}_C$ is computed over $\Delta t = t_1 - t_0$ from Eqs. (23.2) and (23.3) as follows: Let j = Integer($\Delta t/\Delta t_{att}$), $\tau_i = t_0 + i\,\Delta t_{att}$ and do the following

For i = 1, …, j plus final step from τ_j to t_1

$$\widetilde{SV}_C(\tau_i) = \widetilde{SV}_C(\tau_{i-1}) + \dot{\widetilde{SV}}_C(\tau_{i-1})\Delta t_{att} \quad (23.4)$$

At the start of Kalman filter

$(\widetilde{SV}_C, x_{corr}, \dot{x}_{corr}) = (0_3, 0_3, 0_3)$ and $\dot{\widetilde{SV}}_C(t_0) = \dot{SV}_{ACF}(t_0)$ from Eq. (23.2).

At KF re-initialization (see Fig. 5)

$\widetilde{SV}_C(t_0) = \widetilde{SV}_C(t_1)$ from Eq. (23.4) and $\dot{\widetilde{SV}}_C(t_0) = \dot{\widetilde{SV}}_C(t_1)$ from Eq. (23.3)

Note that $\dot{x}_{corr}$ in Eq. (23.3) compensates for IMU drift effect on $\dot{SV}_{ACF}$ of Eq. (23.2).

3.9 KF Detailed Computation (for each data block)

Level 1A data block is searched for landmarks and if there are no landmarks found within the data block, go to the end of the block (item b below). If landmarks (e.g., a total of LM_T) are found, the location (E_{LRF}, N_{LRF}) of each determined landmark is time tagged, e.g., in coordinated universal time (UTC). In view of Fig. 5, the KF propagation process starts from (t_0, x_0^+, P_0^+) of the last event prior to the data block to the first (t_1, x_1^-, P_1^-) within the data block followed by SV_{INR} and ΔZ computations. If ΔZ is acceptable, proceed to (t_1, x_1^+, P_1^+) estimation and KF re-initialization at t_l. This is repeated for all landmarks within the level 1A data block as follows

a. For k=1 to LM_T do to ENDFOR

$t_1 =$ UTC_k at landmark number k, $\Delta t = t_1 - t_0$

Propagation: From step 1 of section 3.1.

INR SV (SV_{INR}): From step 2 of section 3.1.

Residuals ΔZ: From step 3 of section 3.1.

Estimation: From step 4 of section 3.1.

Re-initialize KF at t_l: From step 5 of section 3.1.

ENDFOR

b. At end of data block, do the following

$t_l = UTC_{end}$ at end of data block, $\Delta t = t_1 - t_0$

Propagation: From step 1 of section 3.1.

Re-initialize KF at t_l

$(t_0,\ x_0^+,\ P_0^+) = (t_1, x_1^+,\ P_1^+) = (t_1, x_1^-,\ P_1^-)$.

If maneuver delta V is provided by FDS

c. At maneuver, do the following

t_l= $UTC_{maneuver}$ at maneuver time, $\Delta t = t_1 - t_0$

Propagation: From step 1 of section 3.1.

Re-initialize KF at t_l

$(x_1^+, P_1^+) = (x_1^-, P_1^-) + (\Delta x, \Delta P)$

$\Delta x = R_{Si}^{-1}\left[0_{1x9}\ \ \Delta v_{FDS,r}\ \ \Delta v_{FDS,\lambda}\ \ \Delta v_{FDS,L}\ \ 0_{1x2m}\right]^T$

ΔP diagonal terms 10 to 12 are obtained from Δv errors.

$(t_0,\ x_0^+,\ P_0^+) = (t_1, x_1^+,\ P_1^+)$.

If orbit is provided by FDS instead of delta V

d. At orbit determination (OD), do the following

t_l= UTC_{OD} at OD time, $\Delta t = t_1 - t_0$

Propagation: From step 1 of section 3.1.

Re-initialize KF at t_l

$(x_1^+, P_1^+) = (x_1^-, P_1^-) + (\delta x, \delta P)$

$\delta x = [0_{1x6}\ \ \Delta R_{FDS}/R_{Si}\ \ \Delta\lambda_{FDS}\ L_{FDS}\ 0_{1x3}\ \ 0_{1x2m}]^T_{\text{before OD}}$

$\quad -[0_{1x6}\ \ \Delta R_{FDS}/R_{Si}\ \ \Delta\lambda_{FDS}\ L_{FDS}\ 0_{1x3}\ \ 0_{1x2m}]^T_{\text{after OD}}$

Note that δx is selected to avoid jumps in Eq. (3.1) at OD.

δP diagonal terms 7 to 9 and 12 are obtained from OD errors.

$(t_0,\ x_0^+,\ P_0^+) = (t_1, x_1^+,\ P_1^+)$.

3.10 Thermoelastic Model Time Series

The thermoelastic effects are caused by the apparent motion of the sun around the spacecraft which repeats daily with a slow seasonal variation. This suggests modeling (SV_{corr}, SV_m) of Eqs. (1.3) and (1.7) by, e.g., 15th order Fourier series with one solar day fundamental period like that used by Kamel for GOES I-M [see Sects. 4.3 and 4.6 of Ref. [3] and Eq. (1) of US patent #602391].

The following are additional two approaches to determine time series for $(SV_{corr,model}, SV_{m,model})$, e.g., once/day

1. represent $(SV_{corr,model}, SV_{m,model})$ by Fourier series and use off-line least squares to determine the Fourier series coefficients from previous 7 days of (SV_{corr}, SV_m) data. The results are then used to generate the next day $(SV_{corr,model}, SV_{m,model})$ time series.
2. seven-day average of (SV_m, SV_{corr}) data
   a. create uniform time series at, e.g., one-minute interval using interpolation of original (SV_{corr}, SV_m) time series.
   b. the uniform time series are then used to generate the next day $(SV_{corr,model}, SV_{m,model})$ time series as follows

   For i= 1, 2, ···, 1440, compute the 8^{th} day models from previous 7 days state vectors

$$SV_{corr,model}\,(t_{i,8}) = \frac{1}{7}\sum_{n=1}^{n=7} SV_{corr}(t_{i,n}),\; SV_{m,model}\,(t_{i,8}) = \frac{1}{7}\sum_{n=1}^{n=7} SV_{m}\,(t_{i,n}) \qquad (24)$$

Note that $(SV_{corr,model}, SV_{m,model})$ are initially set to $(0_3, 0_m)$ at the start of KF. Note also that (x_{corr}, x_m) should be adjusted to avoid jumps in Eqs. (1.3) and (1.7) at the transition time from old time series to new time series (e.g., at midnight or OD time). Also, $(SV_{corr,model}, SV_{m,model})$ are uploaded daily for IMC on-board Spacecraft [1].

4 INR Improvement for Single Mirror Instruments

The use of Eq. (16.6) instead of the classical $SV_m = [\phi_m \;\; \theta_m]^T$ in GOES I-M and MTSAT-1R type instruments is expected to improve INR performance and could have improved GOES I-M and MTSAT-1R INR performance if it was available at that time.

4.1 GOES I-M Type Instruments

The yaw misalignment ψ_m has insignificant effect because the visible array dimension is 1 km x 8 km and the IR array dimension is 4 km x 8 km (see pages 28 and 29 of Ref. [21]). Therefore, using Eqs. (16.5) and (16.6) with (A, B) = (56, 112) μrad, a misalignment yaw ψ_m =1000 μrad produces (EW, NS) errors = (ΔE, ΔN) ≈ (0.112,0.056) μrad which are insignificant. On the other hand, the orthogonality O_m due to thermal variation and/or bias of 500 μrad produces large NS star measurement residual error = O_m Tan E ≈ 100 μrad (= 30% of O_m) at E = 11° and NS landmark measurement residual error = O_m Tan E ≈ 75 μrad at E = 8.7° . This error has small effect on frame-to-frame registration but has significant effect (≈150 μrad = 30% of O_m) on within frame registration. The secondary orthogonality misalignments (O_{m1}, O_{m2}) thermal variation and/or bias of 500 μrad produces smaller EW and NS errors because their effects on INR performance is multiplied by (1-C_E) and (1-C_N). This suggests that Kalman Filter INR software design should be based on deleting ψ_m, O_{m1} and/or O_{m2} if proven to be insignificant by analysis and/or during In Orbit Test (IOT).

4.2 MTSAT-1R Type Instruments

MTSAT-1R FPM dimension is about 26 km x 336 km (see Fig. 5 in Ref. [22]). Therefore, Therefore, using Eqs. (16.5) and (16.6) with (A, B) = (364, 4704) μrad and ψ_m = 1000 μrad produces (ΔE, ΔN) ≈ (4.7, 0.4) μrad errors. The orthogonality and the secondary orthogonality angles (O_m, O_{m1}, O_{m2}) produce the same errors described in Sect. 4.1.

During MTSAT-1R IOT, large residual errors between the actual INR measurements and their predicted values led to unsatisfactory imagery products. Many hypotheses were advanced to explain these errors during rigorous, extensive testing and analysis of the daily landmark residual plots led by Mr. Seiichiro Kigawa of Japan Meteorological Agency (JMA). This analysis concluded the existence of systematic errors, but none led to effective correction. To minimize cost and schedule delays of a protracted investigation, ParSEC method was developed and later patented [23] that could remove these systematic errors without the need to know their origin. In this new method, the various residual

errors are modeled in terms of a power series whose coefficients are determined by a least squares algorithm to minimize the landmark residuals. The ParSEC algorithm corrects the detected East and North scan angles (E, N) from a distorted raw image into a non-distorted (E′, N′) space as

$$(E', N') = (E, N) - (\Delta E, \Delta N) \quad (25.1)$$

$$\Delta E = A_0 + A_1 E + A_2 N + A_3 EN + A_4 E^2 + A_5 N^2 \quad (25.2)$$

$$\Delta N = B_0 + B_1 E + B_2 N + B_3 EN + B_4 E^2 + B_5 N^2 \quad (25.3)$$

Where

(E, N) = Instrument (EW, NS) scan angles from raw image

(ΔE, ΔN) = ParSEC (EW, NS) correction angles

(E′, N′) = ParSEC (EW, NS) corrected scan angles

(A_i, B_i) = (ΔE, ΔN) power series i^{th} ParSEC coefficient

The navigation solution residuals after implementation of this method were typically about 14 μrad for stars (~1 raw visible star sense pixel), 20 μrad for visible landmarks (~2/3 visible image pixel), and 40 rad for IR landmarks (~1/3 IR image pixels), which were consistent with expected INR performance. Recently, the ParSEC algorithm was also used in Ref. [24] to improve INR performance.

Note that some of the terms in Eqs. (25.2) and (25.3) are covered by the improved misalignment Eqs. (16.5) and (16.6) (using $\cos x \cong 1 - x^2/2$, $\sin x \cong x$) and were not covered by the first two columns of Eq. (16.5) that was available at MTSAT-1R time. Most likely, these were the unknown source of the systematic errors. If this is the case, the improved misalignment Eqs. (16.5) and (16.6) could eliminate future need for the ParSEC algorithm.

5 Conclusion

Improved image navigation algorithms are presented using KF to determine attitude correction angles, orbit, and instrument misalignments using landmark measurements and orbit maneuvers delta V (or orbit with coarse accuracy) provided by FDS. Application to systems with star and landmark measurements and systems with star only measurements are also presented. The use of the presented improved algorithms is shown to significantly improve the INR performance for single mirror instruments like those used for GOES I-M and MTSAT-1R and for two mirror instruments like the ABI used for GOES-R.

References

1. Kamel AA (2018) Generalized Image Navigation and Registration Algorithms for Ground and Space Segments, Trans. JSASS Aerospace Tech. Japan, Vol. 16 Issue 6, pp. 572-581.
2. Kamel AA (2019) Improved Instrument Misalignment Equations for Image Navigation and Registration (INR), EuroGNC 2019.
3. Kamel AA (1996) GOES Image Navigation and Registration System, Proc. SPIE.
4. Lu F, Zhang X, Xu J (2008) Image Navigation for the FY2 Geosynchronous Meteorological Satellite, J. Atmospheric and Oceanic Technology.

5. Kim H, Harris J (2010) COMS INR; Prospect and Retrospect, Proceedings of the 61st IAC (International Astronautical Congress), Vol. 9, Prague.
6. Chambon T, Soulignac V, Olivier F, and Tanguy P (2013) On-ground Evaluation of MTG Image Navigation and Registration (INR) Performances, Proc. SPIE.
7. Okuyama A, Andou A, Date K, Hoasaka K, Mori N, Murata H, Tabata T, Takahashi M, Yoshino R, and Bessho K (2015) Preliminary Validation of Himawari-8/AHI Navigation and Calibration, Proc. SPIE.
8. Kamel AA, Kim H, Yang D, Park C, and Woo J (2017) Generalized Image Navigation and Registration Method Based on Kalman Filter, Advances in Aerospace Guidance, Navigation, and Control, Springer International Publishing.
9. Kamel AA (1999) Precise Spacecraft Camera Image Navigation and Registration, US patent #5,963,166.
10. Carr JL (2009)Twenty-five years of INR, The J. Astronautical sciences.
11. Harris J, Kamel A, and Kim H (2009) Image Navigation and Registration Improvements using GPS, Proceedings of the 2009 IEEE International Geoscience and Remote Sensing Symposium, Vol. 3, pp. 247-250.
12. De Luccia FJ, Houchin S, Porter BC, Graybill J, Hass E, Johnson PD, Isaacson PJ, and Reth AD (2016) Image Navigation and Registration Performance Assessment Tool Set for the GOES-R Advanced Baseline Imager and Geostationary Lightning Mapper, Proc. SPIE.
13. Griffith PC (2015) Advanced Himawari Imager (AHI) Design and Operational Flexibility, Proceedings of Sixth Asia/Oceania Meteorological Satellite Users' Conference, Tokyo, Japan. http://www.data.jma.go.jp/mscweb/en/aomsuc6_data/oral/s02-01.pdf
14. Gibbs BP, Carr JL (2014) GOES-R Orbit and Instrument Attitude Determination, Proceedings of 24th International Symposium on Space Flight Dynamics, Laurel.
15. Chapel J, Stancliffe D, Bevacqua T, Winkler S, Clapp B, Rood T, Gaylor D, Freesland D, and Krimchansky A (2015) Guidance, navigation, and control performance for the GOES-R spacecraft, CEAS Space Journal, pp. 87–104. https://link.springer.com/article/10.1007%2Fs12567-015-0077-1
16. GOES-R Product Definition and User's Guide (Pug), Vol. 5, DCN-7035538, Revision E, Prepared by Harris Corporation for NASA/NOAA, 02 March 2017. http://www.goes-r.gov/products/docs/PUG-L2+-vol5.pdf
17. Virgilio V N (2015) Geolocation of Remotely Sensed Pixels by Introspective Landmarking, US patent #8,942,421.
18. GOES Earth Location User's Guide (ELUG), DRL 504-11 Revision 1, Appendix C, NOAA, March 1998.
19. Wertz JR (1978) Spacecraft Attitude Determination and Control, D. Reidel Publishing, Hingham, Mass, reprinted in 2000 by Kluwer Academic Publisher, Boston, Mass. pp. 269,461-465 and 764.
20. Ardema MD (2005) Analytical Dynamics Theory and Applications, Kluwer Academic/Plenum Publishers, New York. Page 217.
21. GOES I-M Data Book Prepared by Space Systems/Loral for NASA (1996) https://goes.gsfc.nasa.gov/text/goes.databook.html
22. Puschell JJ et al (2003) Japanese Advanced Meteorological Imager (JAMI) Design, Characterization and Expected On-Orbit Performance. http://cimss.ssec.wisc.edu/itwg/itsc/itsc13/proceedings/posters/a28_puschell.pdf
23. Kamel AA, Sheffield J, Mclaren M (2012) Image navigation and registration accuracy improvement using parametric systematic error correction, United States Patent No. 8301377. https://patentimages.storage.googleapis.com/17/1c/9e/762c11599efcd6/US8301377.pdf
24. Lyu W, Wang T, Dong Y, and Shen Y (2017) Imaging Navigation and Registration for Geostationary Imager, IEEE Geoscience and Remote Sensing letters.